PHYSICAL REVIEW FLUIDS **1**, 052101(R) (2016)

Singular effective slip length for longitudinal flow over a dense bubble mattress

Ory Schnitzer
Department of Mathematics, Imperial College London, South Kensington Campus, London SW7 2AZ, United Kingdom
(Received 27 June 2016; published 13 September 2016)

We consider the effective hydrophobicity of a periodically grooved surface immersed in liquid, with trapped shear-free bubbles protruding between the no-slip ridges at a $\pi/2$ contact angle. Specifically, we carry out a singular-perturbation analysis in the limit $\epsilon \ll 1$ where the bubbles are closely spaced, finding the effective slip length (normalized by the bubble radius) for longitudinal flow along the ridges as $\pi/\sqrt{2\epsilon} - (12/\pi)\ln 2 + (13\pi/24)\sqrt{2\epsilon} + o(\sqrt{\epsilon})$, the small parameter ϵ being the planform solid fraction. The square-root divergence highlights the strong hydrophobic character of this configuration; this leading singular term (along with the third term) follows from a local lubrication-like analysis of the gap regions between the bubbles, together with general matching considerations and a global conservation relation. The $O(1)$ constant term is found by matching with a leading-order solution in the outer region, where the bubbles appear to be touching. We find excellent agreement between our slip-length formula and a numerical scheme recently derived using a unified-transform method [Crowdy, IMA J. Appl. Math. **80**, 1902 (2015)]. The comparison demonstrates that our asymptotic formula, together with the diametric dilute-limit approximation [Crowdy, J. Fluid Mech. **791**, R7 (2016)], provides an elementary analytical description for essentially arbitrary no-slip fractions.

DOI: 10.1103/PhysRevFluids.1.052101

I. INTRODUCTION

There is great current interest in the design and application of microstructured metasurfaces that are effectively superhydrophobic [1–5]; flows varying on scales large compared with the microstructure appear to slip over the surface, rather than satisfy a no-slip condition. A wide body of theoretical literature now exists covering general properties [6–8], along with computations and analytic results for the effective slip length of specific microstructured geometries and materials [9–14]. Building on the pioneering solutions of Phillip [15], a plethora of new results have recently been obtained using complex-variable techniques, in particular conformal mappings [16,17] and the unified-transform method [18,19]. The available numerical and analytical solutions have been further extended by regular-perturbation schemes for nearly flat meniscuses, nearly-shear-free inclusions, and well-separated microstructured elements [20,21].

A prevalent realization of a superhydrophobic surface consists of a periodically grooved solid surface immersed in water, with trapped-air pockets protruding between the solid ridges. For this configuration, sometimes termed a bubble mattress [16], the effective slip length diverges with vanishing solid fraction ϵ (at least as long as the air bubbles remain stably trapped). According to the scalings suggested by Ybert *et al.* [6], this divergence is logarithmic, i.e., for $\epsilon \ll 1$ the slip length is commensurate with the product of the periodicity and $\ln(1/\epsilon)$; for macroscopic flows varying on a scale much larger than the surface periodicity, this implies an inherently weak hydrophobic effect. Fortunately, numerical computations hint that the logarithmic scaling breaks down when the meniscuses of the protruding bubbles are appreciably nonflat. In particular, for longitudinal flow along the cylindrical bubbles, plots of the slip length against bubble separation depict a rapid growth with vanishing separation [11,22]. This is most pronounced in the case of a $\pi/2$ contact angle (see Fig. 12 in Ref. [19]). In this paper we carry out an asymptotic analysis of the small-solid-fraction

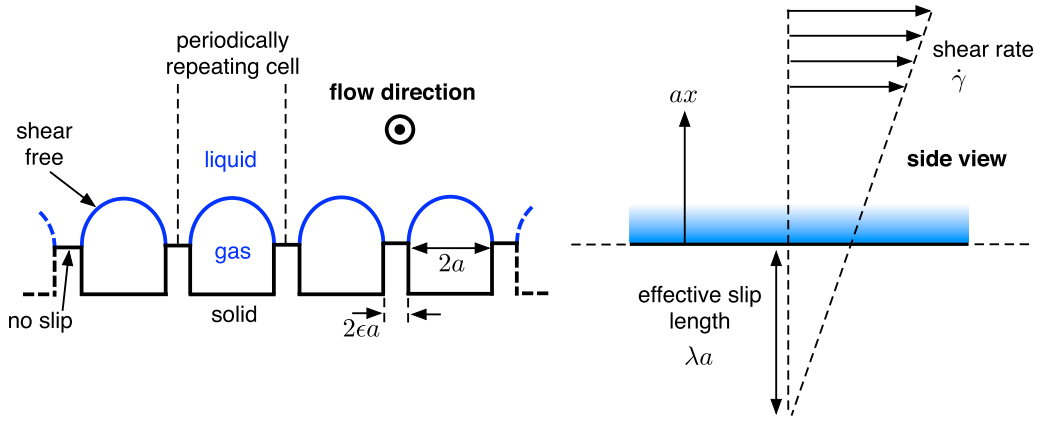

FIG. 1. Schematic of the slip-length problem for longitudinal flow over a bubble mattress.

limit $\epsilon \to 0$ for $\pi/2$ contact angles. Our goal is to derive an accurate asymptotic expansion for the effective slip length and thereby highlight the surprisingly large slip lengths attainable with densely grooved surfaces.

II. PROBLEM FORMULATION

A schematic of the problem is shown in Fig. 1. A periodic array of cylindrical shear-free bubble protrusions (radius a and contact angle $\pi/2$), separated by flat no-slip solid boundaries of thickness $2\epsilon a$, is exposed to a shear flow (shear rate $\dot\gamma$) parallel to the cylindrical bubbles; we assume small capillary numbers and accordingly approximate the bubble cross-sectional boundaries by semicircles. For unidirectional flow parallel to the applied shear and in the absence of a pressure gradient, the flow velocity satisfies Laplace's equation and at large distances is $\sim\dot\gamma a(x+\lambda)$, ax being the normal distance from the solid segments and $a\lambda$ the effective slip length [16]. The problem is periodic and it is sufficient to consider a single unit cell of width $2a(1+\epsilon)$.

We adopt a dimensionless formulation where lengths are normalized by a and velocities by $\dot\gamma a$ and define a Cartesian coordinate system (x,y), where y is measured from the center of an arbitrarily chosen bubble. The unit-cell domain $\mathcal{D}$ is thus bounded by $y=\pm(1+\epsilon)$, the bubble interface $\mathcal{B}$, and the flat solid boundaries $\mathcal{S}$. The problem governing the longitudinal velocity component w is depicted in Fig. 2 and consists of Laplace's equation

$$\nabla^2 w = 0 \quad \text{in } \mathcal{D}, \tag{1}$$

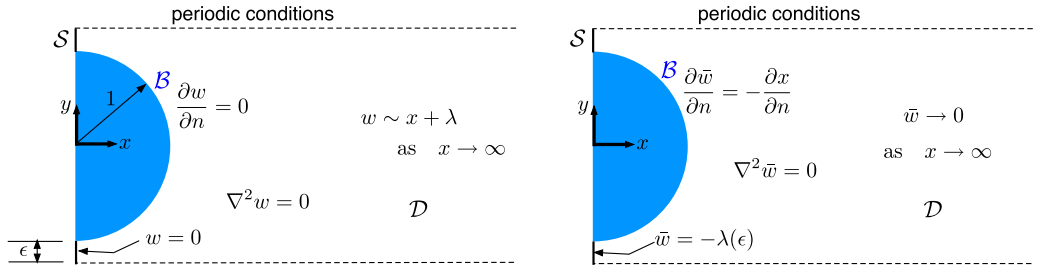

FIG. 2. Shown on the left is the dimensionless formulation. The normalized slip length $\lambda(\epsilon)$ is an outcome of the solution to the boundary value problem. Shown on the right is the formulation in terms of the disturbance velocity $\bar w = w - x - \lambda$.

the no-shear condition

$$\frac{\partial w}{\partial n} = 0 \quad \text{on } \mathcal{B}, \tag{2}$$

the no-slip condition

$$w = 0 \quad \text{on } \mathcal{S}, \tag{3}$$

the far field condition

$$w \sim x + \lambda + o(1) \quad \text{as } x \to \infty, \tag{4}$$

and periodic boundary conditions at $y = \pm(1+\epsilon)$. Since $w(y) = w(-y)$ in $\mathcal{D}$ the latter can be equivalently replaced by the Neumann conditions

$$\frac{\partial w}{\partial y} = 0 \quad \text{at } y = \pm(1+\epsilon). \tag{5}$$

It will prove useful to also keep in mind the integral relation

$$\int_1^{1+\epsilon} \left.\frac{\partial w}{\partial x}\right|_{x=0} dy = 1 + \epsilon, \tag{6}$$

which is readily derived by integrating Laplace's equation (1) over $\mathcal{D}$ and applying the divergence theorem. Physically, (6) represents the fact that in the absence of a longitudinal pressure gradient or body force the shear force away from the surface is the same as that acting on its solid segments. In what follows, it is helpful to alternatively interpret (6) as an integral conservation law with respect to the fictitious irrotational flow ∇w.

In Eq. (4) the first term corresponds to the prescribed shear, whereas $\lambda(\epsilon)$ is unknown. Our goal is thus to determine $\lambda(\epsilon)$ in the limit $\epsilon \to 0$. First, however, we reformulate the problem in terms of the disturbance velocity $\bar{w} = w - x - \lambda$, which turns out to be convenient for the asymptotic analysis. The new problem, also depicted in Fig. 2, is similar to that governing w, but with condition (2) replaced by

$$\frac{\partial \bar{w}}{\partial n} = -\frac{\partial x}{\partial n} \quad \text{on } \mathcal{B}, \tag{7}$$

condition (3) by

$$\bar{w} = -\lambda(\epsilon) \quad \text{on } \mathcal{S}, \tag{8}$$

and (4) by

$$\bar{w} \to 0 \quad \text{as } x \to \infty. \tag{9}$$

Finally, in terms of $\bar{w}$, the integral relation (6) becomes

$$\int_1^{1+\epsilon} \left.\frac{\partial \bar{w}}{\partial x}\right|_{x=0} dy = 1. \tag{10}$$

III. CLOSELY SPACED BUBBLES

A. Singular scaling of the effective slip length

Henceforth we consider the asymptotic limit where $\epsilon \to 0$. We expect the normalized slip length λ to diverge in this limit, but at what rate? The integral relation (10) shows that, for arbitrarily small ϵ, there is a finite $O(1)$ flux $\nabla\bar{w}$ through the solid boundaries $\mathcal{S}$. Noting that the width of those boundaries is $O(\epsilon)$ and adjacent to them $\bar{w} = O(\lambda)$ [cf. (8)], this implies that $\epsilon\lambda/\delta = O(1)$, where δ is the length scale on which $\bar{w}$ varies in the x direction close to $\mathcal{S}$. The latter subdomain of $\mathcal{D}$ is geometrically narrow; in particular, owing to the locally parabolic boundary shape, the

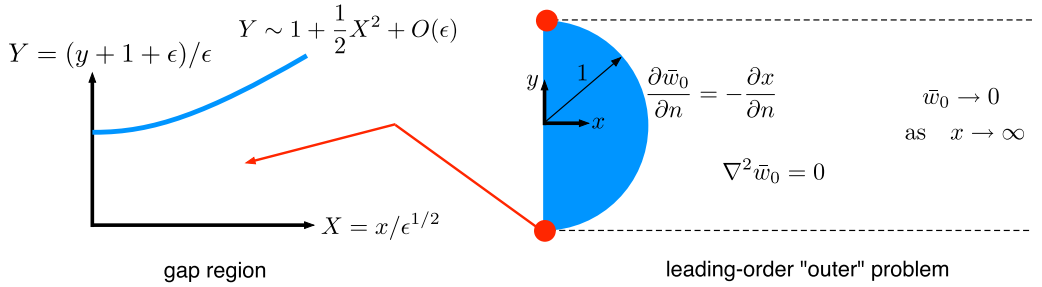

FIG. 3. Shown on the left are the stretched coordinates used to analyze the gap region. Shown on the right is the leading-order outer problem. Matching with the gap regions is required in the limits where $(x,y) \to (0,\pm 1)$ from within the outer liquid domain.

separation between the bubbles remains $O(\epsilon)$ for $x = O(\epsilon^{1/2})$. This implies that $\bar{w}$ is approximately independent of y there and that the right-hand side of (7) is small; thus the product of $d\bar{w}/dx$ and the gap thickness is conserved [cf. (21)]. However, the locally parabolic geometry means that the relative thickness variation is $O(1)$ over a length scale $\epsilon^{1/2}$, i.e., $\delta = O(\epsilon^{1/2})$. It follows that λ and hence $\bar{w}$ in the region between the nearly touching bubbles both scale like $\epsilon^{-1/2}$.

B. Inner gap and outer bubble-scale expansions

The above discussion implies that the asymptotics of $\bar{w}$ as $\epsilon \to 0$ are spatially nonuniform. Accordingly, we conceptually decompose the liquid domain into two inner gap regions, at distances $O(\epsilon^{1/2})$ from the $O(\epsilon)$-thick solid boundaries, and an outer region away from the gaps, where to leading order the bubbles appear to be touching (see Fig. 3). In preparation for our analysis of the inner region (say, in $y < 0$), we define the stretched gap coordinates

$$Y = (y+1+\epsilon)/\epsilon, \quad X = x/\epsilon^{1/2}, \tag{11}$$

in which terms the bubble boundary is $Y = H(X) \sim H_0(X) + \epsilon H_1(X) + o(\epsilon)$, where $H_0 = 1 + \frac{1}{2}X^2$ and $H_1 = X^4/8$, and a gap disturbance velocity $\bar{W}(X,Y) = \bar{w}(x,y)$. The inner problem governing $\bar{W}$ consists of Laplace's equation

$$\epsilon \frac{\partial^2 \bar{W}}{\partial X^2} + \frac{\partial^2 \bar{W}}{\partial Y^2} = 0 \quad \text{for } 0 < Y < H(X),\ X > 0, \tag{12}$$

together with the conditions

$$\bar{W} = -\lambda(\epsilon) \quad \text{at } X = 0, \tag{13}$$

$$\frac{\partial \bar{W}}{\partial Y} = 0 \quad \text{at } Y = 0, \tag{14}$$

and

$$\frac{\partial \bar{W}}{\partial Y} - \epsilon \frac{dH}{dX}\frac{\partial \bar{W}}{\partial X} - \epsilon^{3/2}\frac{dH}{dX} = 0 \quad \text{at } Y = H(X). \tag{15}$$

In addition, $\bar{W}$ must match with the outer region as $X \to \infty$. Recall that we also have at our disposal the global relation (10), which now reads

$$\epsilon^{1/2} \int_0^1 \left.\frac{\partial \bar{W}}{\partial X}\right|_{X=0} dY = 1. \tag{16}$$

In agreement with the scaling arguments given before, it follows from (16) that $\bar{W} = O(\epsilon^{-1/2})$, suggesting the gap expansion

$$\bar{W} \sim \bar{W}_{-1/2}\epsilon^{-1/2} + \bar{W}_0 + \epsilon^{1/2}\bar{W}_{1/2} + \epsilon\bar{W}_1 + \epsilon^{3/2}\bar{W}_{3/2} + \cdots; \tag{17}$$

condition (13) then confirms the scaling $\lambda = O(\epsilon^{-1/2})$ and we anticipate the expansion

$$\lambda \sim \lambda_{-1/2}\epsilon^{-1/2} + \lambda_0 + \lambda_{1/2}\epsilon^{1/2} + \cdots. \tag{18}$$

The gap problem at each order is found by substitution of (17) into (12)–(16) and by mapping (15) onto the nominal surface $Y = H_0(X)$ by means of a Taylor expansion in Y; in particular, it is readily seen from (12) and (14) that $W_{-1/2}$ and W_0 are independent of Y, namely, $W_{-1/2} = W_{-1/2}(X)$ and $W_0 = W_0(X)$.

In the outer region we anticipate, subject to confirmation through matching, that the disturbance velocity is $O(1)$. We accordingly expand $\bar{w}$ as

$$\bar{w} \sim \bar{w}_0 + o(1), \quad \bar{w}_0 = O(1), \tag{19}$$

where the leading-order outer problem governing $\bar{w}_0$ is shown in Fig. 3. The depicted domain is bounded by the two rays $y = \pm 1$ $(x > 0)$ and the semicircle $x^2 + y^2 = 1$ $(x > 0)$; the error incurred by mapping the boundary conditions on $y = \pm(1+\epsilon)$ to $y = \pm 1$ is small in ϵ and accordingly does not enter the leading-order problem. Thus, the outer disturbance velocity $\bar{w}_0$ satisfies Laplace's equation, attenuation as $x \to \infty$, periodicity at $y = \pm 1$, and a boundary condition identical to (7) on the half circle. The boundary of the leading-order outer region is nonsmooth where the rays and semicircle coincide; at these points $\bar{w}_0$ is allowed to be singular, the only requirement being that matching with the gap region is satisfied.

C. Leading-order asymptotics

Consider the gap region. Laplace's equation (12) at $O(\epsilon^{1/2})$ reads

$$\frac{d^2\bar{W}_{-1/2}}{dX^2} + \frac{\partial^2\bar{W}_{1/2}}{\partial Y^2} = 0. \tag{20}$$

Integrating with respect to Y between 0 and $H_0(X)$, together with the appropriate asymptotic orders of (14) and (15), yields

$$\frac{d}{dX}\left(H_0\frac{d\bar{W}_{-1/2}}{dX}\right) = 0; \tag{21}$$

this is precisely the flux conservation law anticipated in Sec. III A. Integrating, in conjunction with the conditions

$$\bar{W}_{-1/2} = -\lambda_{-1/2}, \quad \frac{d\bar{W}_{-1/2}}{dX} = 1 \quad \text{at } X = 0, \tag{22}$$

which respectively follow from (13) and (16), we find

$$\bar{W}_{-1/2} = \sqrt{2}\arctan\frac{X}{\sqrt{2}} - \lambda_{-1/2}. \tag{23}$$

Consider now the far-field behavior of (23),

$$\bar{W}_{-1/2} \sim \frac{\pi}{\sqrt{2}} - \lambda_{-1/2} - \frac{2}{X} + O\left(\frac{1}{X^3}\right) \quad \text{as } X \to \infty. \tag{24}$$

According to van Dyke's matching rule [23], the constant leading-order term in Eq. (24) implies an $O(\epsilon^{-1/2})$ disturbance velocity in the outer region, forced solely by the condition that it approaches $\pi/\sqrt{2} - \lambda_{-1/2}$ in the limit where $(x, y) \to (0, \pm 1)$ from within the outer liquid domain. The only such solution, however, is constant everywhere, contradicting the far-field condition that $\bar{w}$ attenuates

as $x \to \infty$. It follows that there cannot be an $O(\epsilon^{-1/2})$ term in the outer region, thereby confirming assumption (19) [cf. (27)] and showing that

$$\lambda_{-1/2} = \frac{\pi}{\sqrt{2}}. \tag{25}$$

D. Leading-order correction

It is readily found that the gap correction $\bar{W}_0$ is governed by an equation identical to (21). It follows that

$$\bar{W}_0 = C \arctan \frac{X}{\sqrt{2}} - \lambda_0, \tag{26}$$

but since the global relation (16) is trivial at $O(\epsilon^{1/2})$, $C = 0$. The leading correction to the slip length λ_0 is determined as follows. On the one hand, given (24) and (26), van Dyke's matching rule shows that the leading-order outer field satisfies

$$\bar{w}_0 \sim -\frac{2}{x} - \lambda_0 + o(1) \quad \text{as } (x, y) \to (0, \pm 1). \tag{27}$$

On the other hand, the outer-region problem governing $\bar{w}_0$, shown in Fig. 3, is closed by the lower-order matching condition $\bar{w}_0 \sim -2/x$. Thus once $\bar{w}_0$ is solved for, the slip-length correction can be found as $\lambda_0 = -\lim_{x\to 0}(\bar{w}_0 + 2/x)$. In the Appendix we solve the outer problem using a conformal mapping, finding

$$\lambda_0 = -\frac{12}{\pi} \ln 2 \approx -2.648. \tag{28}$$

E. First-order correction

Turning again to the inner region, integration of (20) together with the $O(\epsilon^{1/2})$ balance of (14) shows that

$$\bar{W}_{1/2} = \frac{1}{2} \frac{X}{H_0^2(X)} Y^2 + \mathcal{A}(X), \tag{29}$$

where $\mathcal{A}(X)$ is an integration constant. A solvability condition on $\bar{W}_{3/2}$ is derived in the usual way by integrating (12) from $Y = 0$ to $H_0(X)$ while using the $O(\epsilon^{3/2})$ balances of the periodicity condition (14) and the no-shear condition (15), the latter balance being

$$\frac{\partial \bar{W}_{3/2}}{\partial Y} = \frac{dH_1}{dX}\frac{d\bar{W}_{-1/2}}{dX} + \frac{dH_0}{dX}\frac{\partial \bar{W}_{1/2}}{\partial X} - H_1 \frac{\partial^2 \bar{W}_{1/2}}{\partial Y^2} + \frac{dH_0}{dX} \quad \text{at } Y = H_0(X). \tag{30}$$

The resulting solvability condition provides a differential equation governing $\mathcal{A}(X)$; in conjunction with the $O(\epsilon^{3/2})$ and $O(\epsilon^2)$ balances of (13) and (16), respectively, we find the following problem:

$$\frac{d}{dX}\left(H_0 \frac{d\mathcal{A}}{dX}\right) = \frac{2X}{(2 + X^2)^2} - X, \quad \mathcal{A}|_{X=0} = -\lambda_{1/2}, \quad \left.\frac{d\mathcal{A}}{dX}\right|_{X=0} = -1/6. \tag{31}$$

From the solution to this problem it follows that

$$\mathcal{A} \sim -X + \frac{13\pi}{12\sqrt{2}} - \lambda_{1/2} + O\left(\frac{1}{X}\right) \quad \text{as } X \to \infty. \tag{32}$$

The leading term in Eq. (32), along with the leading term in an expansion of the Y-dependent term in Eq. (29), is expected to match with high-order terms in the inner limit of $\bar{w}_0$. The constant term in Eq. (32), however, forces a constant outer-region solution at $O(\epsilon^{1/2})$, which contradicts the

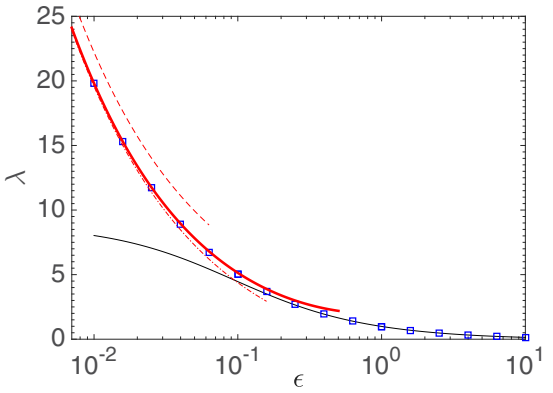

FIG. 4. Slip length normalized by bubble radius, as a function of half the dimensionless minimum separation between the bubbles. The thick line shows the near-contact asymptotics (34), the thin dash-dotted line the two first terms of (34), the thin dashed line the leading singular term of (34), the symbols the numerical solution using the unified-transform method [19], and the thin solid line the dilute-limit approximation [21]; see Sec. IV for details.

attenuation of $\bar{w}$ as $x \to \infty$; note that the deviation of the periodic-cell boundaries from $y = \pm 1$ modifies the outer-region problem only at $O(\epsilon)$. We thus find

$$\lambda_{1/2} = \frac{13\pi}{12\sqrt{2}} \approx 2.407. \tag{33}$$

IV. CORROBORATION AND DISCUSSION

To recapitulate, we have derived the near-contact asymptotics of the effective slip length, normalized by the bubble radius, as

$$\lambda \sim \frac{\pi}{\sqrt{2\epsilon}} - \frac{12}{\pi}\ln 2 + \frac{13\pi}{12\sqrt{2}}\sqrt{\epsilon} + \cdots \quad \text{as } \epsilon \to 0. \tag{34}$$

Figure 4 demonstrates excellent agreement of our asymptotic result with an exact numerical solution obtained using an accurate and efficient scheme derived from the unified-transform method [19]. Also shown is the approximation $\lambda \approx \pi l^{-1}/(2 - \pi^2/6l^2)$, where $l = 1 + \epsilon$, derived in the dilute limit of well-separated bubbles [21]. While the dilute and near-contact limit do not asymptotically overlap, they together provide a rather complete description, for arbitrary ϵ, in terms of elementary expressions. As was pointed out in Ref. [24], the problem considered herein can be mapped using symmetry to the potential-flow problem of calculating the blockage coefficient for potential flow through a slit channel constricted by a circular cylinder. The present asymptotic solution may therefore have ramifications also in electrostatics, flow through porous media, and large-Reynolds-number hydrodynamics.

We have focused in this paper on the case where the contact angle is $\pi/2$. For contact angles appreciably below $\pi/2$, the inner region is no longer narrow, leading to a gap velocity varying over an $O(\epsilon)$ length scale rather than $O(\epsilon^{1/2})$. The divergence of the effective slip length as $\epsilon \to 0$ is then logarithmic in ϵ [6]. A detailed asymptotic analysis of the effective slip length for arbitrary contact angles is beyond the scope of the present paper.

ACKNOWLEDGMENTS

I thank Professor Darren Crowdy for pointing me to Refs. [25,26] for the conformal mapping employed in the Appendix and Elena Luca for sending me a MATLAB code that solves for the

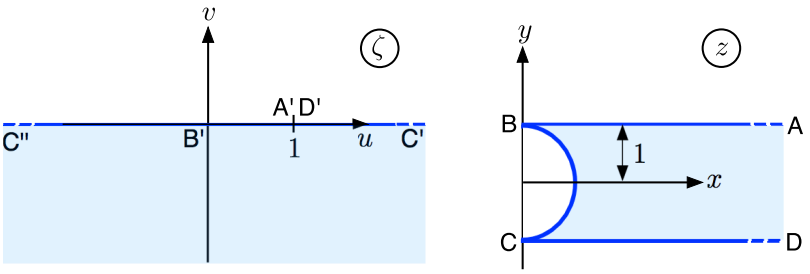

FIG. 5. Conformal mapping employed in the Appendix.

slip length numerically based on a unified-transform method [19], which was used to produce the symbols in Fig. 4. I am also grateful to Ehud Yariv for helpful suggestions and to an anonymous referee that spotted an error in an earlier version of this paper.

APPENDIX: SOLUTION TO THE LEADING-ORDER OUTER PROBLEM

We here solve the leading-order outer problem as shown in Fig. 3, supplemented by the matching condition (27) discussed in Sec. III. As a preliminary step, we introduce a conformal mapping between the lower half of an auxiliary complex plane $\zeta = u + iv$ to the zero-angle curvilinear degenerate triangle in the physical plane $z = x + iy$. Fixing the locations of the critical points on the u axis as depicted in Fig. 5, the required mapping is written as [26]

$$z = i + \frac{2\Lambda(\zeta)}{\Lambda(1-\zeta)}, \tag{A1}$$

where Λ stands for the hypergeometric function

$$\Lambda(\zeta) = F\left(\frac{1}{2},\frac{1}{2},1,\zeta\right) = \frac{1}{\pi}\int_0^1 t^{-1/2}(1-t)^{-1/2}(1-\zeta t)^{-1/2}dt, \tag{A2}$$

with $z^p = \exp[p\log(z)]$, the branch cut of the principle-value logarithm taken along the negative real axis. Note that $\Lambda(\zeta)$ is a single-valued analytical function in the ζ plane excluding the branch-cut ray $u > 1$ along the real axis $v = 0$ [27]. Along this branch cut $\Lambda(\zeta)$ is discontinuous [28],

$$\lim_{\delta\to 0}\Lambda(1+\lambda-i\delta) = \mp i\Lambda(-\lambda) + (1+\lambda)^{-1/2}\Lambda\left(\frac{1}{1+\lambda}\right) \quad \text{for } \delta \gtrless 0, \tag{A3}$$

where $\lambda > 0$ is real; note that $\Lambda(u)$ is real and positive for $u < 1$.

The mapping (A1) is verified as follows. First, note that $\Lambda(u)$, where $0 < u < 1$, is real and positive, ranging from 1 to ∞; it follows that $\Lambda(u)/\Lambda(1-u)$ spans the positive real axis and hence from (A1) that $A'B'$ is mapped to AB (see Fig. 5). Next, using (A3) and (A1) we find

$$\lim_{\delta\to 0} z(1+\lambda-i\delta) = -i + \frac{2\Lambda\left(\frac{1}{1+\lambda}\right)}{(1+\lambda)^{1/2}\Lambda(-\lambda)}, \tag{A4}$$

$$\lim_{\delta\to 0} z(-\lambda-i\delta) = i + \frac{2\Lambda(-\lambda)}{i\Lambda(-\lambda) + (1+\lambda)^{-1/2}\Lambda\left(\frac{1}{1+\lambda}\right)}, \tag{A5}$$

where λ and δ are positive and real. In Eq. (A4) the second term on the right-hand side spans the positive real axis and therefore $C'D'$ (approached from the lower half plane) is mapped to CD. Finally, it is readily verified that the absolute magnitude of (A5) is unity, showing that $B'C''$ is mapped to the semicircle BC.

We now look for a solution in the form $\bar{w}_0 + x = \mathrm{Re}\{T(\zeta)\}$, where T is an analytical function in the half plane $\mathrm{Im}\{\zeta\} < 0$. To this end, we invoke the asymptotic relations [27]

$$\Lambda(\zeta) \sim -\frac{1}{\pi}\log(1-\zeta) + \frac{1}{\pi}\ln 16 + o(1) \quad \text{as } \zeta \to 1,$$
$$\Lambda(\zeta) \sim 1 + o(1) \quad \text{as } \zeta \to 0, \tag{A6}$$

where in the first $|\arg(1-\zeta)| < \pi$; the corresponding behaviors of $\Lambda(1-\zeta)$ as $\zeta \to 0,1$ readily follow. Together with (A1), the above asymptotic relations imply that the far-field condition $\lim_{x\to\infty} \bar{w}_0 = 0$ and the matching condition, that $\bar{w}_0 \sim -2/x$ as $x \to 0$, with $(1-y) \ll x$, are satisfied if

$$T \sim z + o(1) \quad \text{as } \zeta \to 1,$$
$$T \sim -\frac{2}{z-i} + O(1) \quad \text{as } \zeta \to 0. \tag{A7}$$

Employing (A1) and (A6), it is readily verified that an analytic function satisfying (A7) for which $\mathrm{Re}\{T\}$ satisfies Neumann conditions on the domain boundary is

$$T = \frac{1}{\pi}\log\zeta - \frac{2}{\pi}\log(1-\zeta) + i + \frac{8}{\pi}\ln 2. \tag{A8}$$

Inspecting the limit as $\zeta \to 0$ and using (A6), we find

$$\bar{w}_0 \sim -\frac{2}{x} + \frac{12}{\pi}\ln 2 + o(1) \quad \text{as } x \to 0 \quad (y - 1 \ll x), \tag{A9}$$

from which the result (28) follows.

[1] C. Cottin-Bizonne, J.-L. Barrat, L. Bocquet, and E. Charlaix, Low-friction flows of liquid at nanopatterned interfaces, Nat. Mater. **2**, 237 (2003).
[2] C.-H. Choi and C.-J. Kim, Large Slip of Aqueous Liquid Flow over a Nanoengineered Superhydrophobic Surface, Phys. Rev. Lett. **96**, 066001 (2006).
[3] R. Truesdell, A. Mammoli, P. Vorobieff, F. van Swol, and C. J. Brinker, Drag Reduction on a Patterned Superhydrophobic Surface, Phys. Rev. Lett. **97**, 044504 (2006).
[4] J. Hyväluoma and J. Harting, Slip Flow Over Structured Surfaces with Entrapped Microbubbles, Phys. Rev. Lett. **100**, 246001 (2008).
[5] J. P. Rothstein, Slip on superhydrophobic surfaces, Annu. Rev. Fluid Mech. **42**, 89 (2010).
[6] C. Ybert, C. Barentin, C. Cottin-Bizonne, P. Joseph, and L. Bocquet, Achieving large slip with superhydrophobic surfaces: Scaling laws for generic geometries, Phys. Fluids **19**, 123601 (2007).
[7] K. Kamrin and H. A. Stone, The symmetry of mobility laws for viscous flow along arbitrarily patterned surfaces, Phys. Fluids **23**, 031701 (2011).
[8] S. Schmieschek, A. V. Belyaev, J. Harting, and O. I. Vinogradova, Tensorial slip of superhydrophobic channels, Phys. Rev. E **85**, 016324 (2012).
[9] E. Lauga and H. A. Stone, Effective slip in pressure-driven Stokes flow, J. Fluid Mech. **489**, 55 (2003).
[10] A. M. J. Davis and E. Lauga, Geometric transition in friction for flow over a bubble mattress, Phys. Fluids **21**, 011701 (2009).
[11] C. J. Teo and B. C. Khoo, Flow past superhydrophobic surfaces containing longitudinal grooves: effects of interface curvature, Microfluid. Nanofluid. **9**, 499 (2010).
[12] K. Kamrin, M. Z. Bazant, and H. A. Stone, Effective slip boundary conditions for arbitrary periodic surfaces: the surface mobility tensor, J. Fluid Mech. **658**, 409 (2010).

[13] C. Schönecker and S. Hardt, Longitudinal and transverse flow over a cavity containing a second immiscible fluid, J. Fluid Mech. **717**, 376 (2013).
[14] R. Enright, M. Hodes, T. Salamon, and Y. Muzychka, Isoflux Nusselt number and slip length formulae for superhydrophobic microchannels, J. Heat Transfer **136**, 012402 (2014).
[15] J. R. Philip, Flows satisfying mixed no-slip and no-shear conditions, Z. Angew. Math. Phys. **23**, 353 (1972).
[16] D. Crowdy, Slip length for longitudinal shear flow over a dilute periodic mattress of protruding bubbles, Phys. Fluids **22**, 121703 (2010).
[17] D. Crowdy, Frictional slip lengths for unidirectional superhydrophobic grooved surfaces, Phys. Fluids **23**, 072001 (2011).
[18] D. Crowdy, Effective slip lengths for longitudinal shear flow over partial-slip circular bubble mattresses, Fluid Dyn. Res. **47**, 065507 (2015).
[19] D. Crowdy, A transform method for Laplace's equation in multiply connected circular domains, IMA J. Appl. Math. **80**, 1902 (2015).
[20] M. Sbragaglia and A. Prosperetti, A note on the effective slip properties for microchannel flows with ultrahydrophobic surfaces, Phys. Fluids **19**, 043603 (2007).
[21] D. G. Crowdy, Analytical formulae for longitudinal slip lengths over unidirectional superhydrophobic surfaces with curved menisci, J. Fluid Mech. **791**, R7 (2016).
[22] C. Ng and C. Y. Wang, Effective slip for Stokes flow over a surface patterned with two- or three-dimensional protrusions, Fluid Dyn. Res. **43**, 065504 (2011).
[23] E. J. Hinch, *Perturbation Methods* (Cambridge University Press, Cambridge, 1991).
[24] D. Crowdy, Frictional slip lengths and blockage coefficients, Phys. Fluids **23**, 091703 (2011).
[25] S. J. S. Morris, The evaporating meniscus in a channel, J. Fluid Mech. **494**, 297 (2003).
[26] M. J. Ablowitz and A. S. Fokas, *Complex Variables: Introduction and Applications* (Cambridge University Press, Cambridge, 2003).
[27] M. Abramowitz and I. A. Stegun, *Handbook of Mathematical Functions* (Dover, New York, 1972).
[28] Relation (A3) can be derived following Morris [25], who split the integral in Eq. (A2) at $t = 1/(1+\lambda)$ and then wrote the resulting two integrals in terms of hypergeometric functions by changing variables. We note, however, that Morris's derivation ignores the discontinuity, whereby he finds only one of the limits in Eq. (A3); this overlook leads him to incorrectly conclude that his mapping, which, up to a translation, is the same as (A1), should be considered from the upper (rather than lower) half plane.